



Calcium-modified clinoptilolite as a recovery medium of phosphate and potassium from anaerobically digested olive mill wastewater

Dimitris Mitrogiannis¹ · Maria Psychoyou¹ · Michael E. Kornaros² · Konstantina Tsigkou² · Mathieu Brulé¹ · Nikolaos Koukouzas³ · Dimitris Alexopoulos³ · Dimitrios Palles⁴ · Efstratios Kamitsos⁴ · Georgios Oikonomou⁵ · Angeliki Papoutsas¹ · Stamatis Xydous¹ · Ioannis Baziotis¹

Received: 25 March 2019 / Accepted: 29 November 2019 / Published online: 14 December 2019

© Springer-Verlag GmbH Germany, part of Springer Nature 2019

Abstract

Olive mill wastewater (OMW) is characterized as a high-strength effluent due to the high organic load, low biodegradability, and presence of phytotoxic compounds. Most of the OMW treatment methods proposed, including adsorption, focus mainly on the reduction of chemical oxygen demand and recovery of polyphenols. Adsorption studies aiming at nutrient removal from OMW are very limited. In the present work, Ca(OH)₂-treated zeolite (CaT-Z) in a granular form was used for simultaneous recovery of phosphate (PO₄³⁻) and potassium (K⁺) ions from two samples of anaerobically digested OMW. Nutrient adsorption was investigated as a function of contact time, pH and dilution of OMW with deionized water. The lower removal efficiency of phosphorus (P) by CaT-Z was observed at higher dilution ratios consisted of 3.125–6.25% OMW-1 and 5% OMW-2. The maximum P removal was 73.9% in 25% OMW-1 and 85.9% in 10% OMW-2. Potassium removal, as the predominant cation of OMW samples, increased from 17.3 to 46.1% in OMW-1 and from 15.1 to 57.7% in OMW-2 with increasing dilution. The maximum experimental adsorption capacities were 15.8 mg K and 2.14 mg P per gram of CaT-Z. Five sequential treatments of 50% OMW-2 with fresh CaT-Z at each stage ensured a cumulative removal of 87.5% for P and 74.9% for K. Adsorption kinetics were faster for K than for P. The plant-available P was found to be the predominant fraction on the loaded CaT-Z. Electron Probe Microanalysis confirmed the enhanced content of K and P on the loaded CaT-Z, whereas X-ray mapping revealed the co-distribution of Ca and P. This study demonstrates the potential usage of CaT-Z as an immobilization medium of P and K from anaerobically treated OMW.

Keywords Olive mill wastewater · Anaerobic digestion · Zeolite · Phosphate · Potassium · Adsorption

Responsible editor: Philippe Garrigues

Electronic supplementary material The online version of this article (<https://doi.org/10.1007/s11356-019-07212-5>) contains supplementary material, which is available to authorized users.

✉ Dimitris Mitrogiannis
mitrogdimi@gmail.com

¹ Department of Natural Resources Management and Agricultural Engineering, Agricultural University of Athens, 75 Iera Odos, 11855 Athens, Greece

² Laboratory of Biochemical Engineering & Environmental Technology, Department of Chemical Engineering, University of Patras, Rion, GR 26504 Patras, Greece

³ Centre for Research and Technology Hellas (CERTH), Chemical Process and Energy Resources Institute (CPERI), 52 Egialias str., Maroussi, 15125 Athens, Greece

⁴ Theoretical and Physical Chemistry Institute, National Hellenic Research Foundation, 48 Vassileos Constantinou Avenue, 11635 Athens, Greece

⁵ Institute of Geology and Mineral Exploration, Olympic Village Acharnae, 13677 Athens, Greece

Introduction

Mediterranean countries generate substantial volumes of olive mill wastewater (OMW), up to $30 \times 10^6 \text{ m}^3/\text{year}$, through the three-phase olive oil extraction process (Frasconi et al. 2016; Kougias et al. 2014). The effluents are characterized by high chemical oxygen demand (COD), low biodegradability and high quantity of phytotoxic and antimicrobial compounds (Zagklis et al. 2015). These properties constitute a critical economic and environmental issue which led several countries to set legislations about the safe storage, disposal, and spreading of OMW on agricultural fields (Koutsos et al. 2018).

Among various biological, physicochemical or combined treatment methods proposed (Zagklis et al. 2013), the anaerobic digestion of OMW, either as a sole substrate or in co-digestion with other agro-industrial wastewaters, has progressively gained attention in the last decade (Khoufi et al. 2015; Kougias et al. 2014; Maragkaki et al. 2018; Tsigkou et al. 2019). This technique reduces the high organic load, produces biogas and generates a more stabilized liquid digestate with neutral to slightly alkaline pH (Akhlar et al. 2017; Kougias et al. 2014). As such, the digestate has the advantage of being more suitable for agricultural irrigation under specific restrictions (Barbera et al. 2013; Świąteczak et al. 2019). The anaerobically digested OMW may still contain considerable amounts of plant macronutrients. Taking into account the short seasonal operation, wide regional dispersion and small- or middle-scale of olive mill facilities in the producing countries, decentralized and low-cost OMW treatment processes are preferred for full-scale applications. In this context, the adsorption technique comes under consideration as a simple and flexible separation process being part of an integrated OMW treatment system (Frasconi et al. 2016).

It is noteworthy that most of the OMW treatment methods tested in lab-scale, including adsorption, have mainly focused on the COD reduction and recovery of phytotoxic but valuable pollutants like phenolic compounds (Kontos et al. 2014; Zagklis et al. 2015). Removal of the dissolved organics, including polyphenols, by various mineral, biological, and synthetic adsorbents or ion exchangers, has been extensively investigated (Achak et al. 2009a; Al-Malah et al. 2000; Azzam 2018; Frasconi et al. 2016; Víctor-Ortega et al. 2016; Zagklis et al. 2015). The recovery of these organic compounds is of first priority due to the potential generation of valuable by-products as well as their higher concentration in OMW compared with inorganic compounds, such as nitrogen (N) and phosphorus (P) (Achak et al. 2009b; Zagklis et al. 2015). However, a recent work (Pantziaros et al. 2018) investigated the recovery of P from raw OMW by struvite precipitation with the external addition of Mg^{2+} salts and NH_4OH solution, demonstrating the scientific interest in nutrient recovery from OMW.

Adsorption studies aiming at inorganic nutrient recovery from OMW are very limited and have been carried out only on untreated OMW being an acidic effluent. In these studies, nutrients were recovered by sand filter (Achak et al. 2009b) or combined natural materials including clinoptilolite (Aly et al. 2018; Aly et al. 2014). Nutrient capture from OMW in an easily transportable form, such as on abundant, low-cost and soil-friendly mineral matrices, can be favorable for crop fertilization at the desired time, rate and quantity contributing to the goals of a circular and sustainable rural economy (Kocatürk-Schumacher et al. 2017a, b; Koutsos et al. 2018). Moreover, the immobilization of reactive N and P, which mainly occur in the form of ammonium cations (NH_4^+) and phosphate anions (PO_4^{3-}), from various wastewaters onto mineral adsorbents and their application as slow-release fertilizers and soil conditioners can reduce the serious environmental problem of nutrient runoff from agricultural fields following the direct spreading of wastewaters (Kocatürk-Schumacher et al. 2017a, b). To our knowledge, anaerobically digested OMW has not been yet treated through adsorption. Nevertheless, nutrient recovery from the liquid fraction of biogas digestate has gained more attention in recent years due to the increasing number of biogas plants worldwide (Kocatürk-Schumacher et al. 2017a, b; Lin et al. 2014; Wan et al. 2017). Earlier works have employed raw clinoptilolite (Lin et al. 2014, Wan et al. 2017), modified bentonite (Markou et al. 2018) and synthetic zeolite from fly ash (Chen et al. 2012) for P or/and N recovery from various fermentation effluents or biogas digestate. Here, it should be also noted that in contrast to the primary scientific interest in N and P adsorption from wastewaters, the simultaneous potassium (K^+) recovery has been less studied (Kocatürk-Schumacher et al. 2017a, b; Wijesinghe et al. 2018) considering this essential crop nutrient as non-toxic (Aly et al. 2014). However, K^+ is the subject of increasing scientific concerns regarding the effects of K^+ salts accumulation on soil structural stability and hydraulic conductivity as a result of the long-term and repeated disposal of high salinity wastewaters, such as winery and olive mill effluents, especially on clay soils (Arienzo et al. 2012; Barbera et al. 2013; Howell and Myburgh 2018).

In the present study, $\text{Ca}(\text{OH})_2$ -treated zeolite (CaT-Z) was used for nutrient recovery from anaerobically digested OMW characterized by lower initial concentrations of soluble P (around 50 mg/L) than these of the wastewater treated in our previous works (Markou et al. 2018; Mitrogiannis et al. 2018). The main objectives of this work are to test the P adsorption performance of CaT-Z in a treated wastewater type of regional importance in the Mediterranean area and to investigate the P adsorption mechanisms. Another aim is to examine the adsorption of K^+ which is the dominant cation in OMW. Two different samples of anaerobically digested OMW were employed aiming at more reliable results and comparing the adsorption capacities for P and K under varied OMW

chemical properties. Various in situ and bulk instrumental analyses were carried out to determine the nutrient adsorption mechanisms onto CaT-Z. Finally, desorption tests were performed on the spent adsorbent to estimate the speciation of adsorbed P.

Materials and methods

Pretreatment of olive mill wastewater and zeolite

The primary, untreated OMW was collected during the olive oil extraction season of October–December 2016 from a three-phase olive mill in the region of Patras (Western Greece). Adsorption tests were performed using two different samples of anaerobically digested OMW, generated in the Laboratory of Biochemical Engineering and Environmental Technology (LBEET) at the University of Patras. The anaerobic digestion process was carried out in an upflow packed bed reactor (UPBR) operating at 55 °C with a hydraulic retention time (HRT) of 6 days (d). The first sample of 0.75 L (OMW-1) has been stored in a freezer at LBEET until to be sent in March 2017 to the Agricultural University of Athens (AUA), where the adsorption tests took place. The second sample of 1.5 L (OMW-2) remained at room temperature at LBEET for about 4–6 months until to be sent to AUA in October 2017. The experiments with OMW-1 were finished before receiving the OMW-2 sample. At AUA, both samples were stored, after a two-fold dilution with deionized water (DI) (ratio of $V_{DI}/V_{OMW} = 50/50$), in PET (polyethylene terephthalate) bottles and in a fridge (7–9 °C) before and during the experiments. As shown in Table 1, OMW-1 (Fig. 1a) contained more dissolved COD, phenols and other organics than OMW-2 (Fig. 1b). The lower concentrations of organics in OMW-2 can be attributed to its storage at room temperature and the oxidizing or consuming activity of anaerobic microorganisms. As reported for untreated OMW (Achak et al. 2009a; Aharonov-Nadborny et al. 2018; Aly et al. 2014), the major inorganic cation of OMW-1 and OMW-2 was K^+ , whereas P concentrations were within the reported ranges. Both samples were also characterized by low NH_4-N concentrations.

The raw (untreated) natural zeolite (NZ) was sieved to particle size range of 0.5–1.19 mm and pretreated with 0.25 mol/L of technical grade $Ca(OH)_2$. The preparation and pretreatment of NZ are described in earlier works (Mitrogiannis et al. 2017; Mitrogiannis et al. 2018).

Experimental procedure

Batch adsorption runs with OMW-1 and OMW-2 were conducted at temperature (T) of 25 ± 0.5 °C, agitation speed of 200 rpm and adsorbent dosage of 10 g/L. A volume of 20 or

Table 1 Physicochemical characteristics of OMW-1 and OMW-2 prior to adsorption tests (mean \pm standard deviation of n replicates given in parentheses)

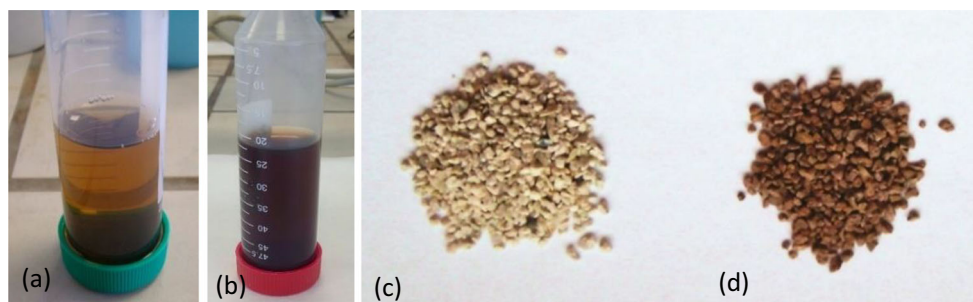
Parameters	OMW-1	OMW-2
pH	7.72 \pm 0.07 ^a (2)	8.30 \pm 0.03 (3)
EC (mS/cm)	5.56 \pm 0.00 (3)	5.48 \pm 0.00 (3)
Total P (mg/L)	–	55.26 \pm 1.70 (2)
Dissolved PO_4-P (mg/L)	48.38 \pm 1.01 (2)	50.05 \pm 0.07 (2)
NH_4-N (mg/L)	16.02 \pm 0.40 (3)	17.36 \pm 0.00 (2)
Total Kjeldahl nitrogen (mg/L)	–	98.0 \pm 9.9 (2)
Na^+ (mg/L)	62.4 \pm 0.0 (2)	131.2 \pm 0.7 (3)
K^+ (mg/L)	1684.2 \pm 5.9 (2)	1708.0 \pm 21.1 (3)
Total alkalinity (g $CaCO_3/L$)	2.0 \pm 0.1 (3)	2.0 (1) ^b
Total COD (g/L)	10.92 \pm 0.94 (3)	3.35 \pm 0.05 (2)
Dissolved COD (g/L)	8.05 \pm 0.07 (3)	3.07 \pm 0.04 (2)
Total carbohydrates (g/L)	0.44 \pm 0.09 (3)	0.18 \pm 0.00 (2)
Dissolved carbohydrates (g/L)	0.31 \pm 0.08 (3)	0.16 \pm 0.00 (2)
Dissolved phenols (g/L)	1.16 \pm 0.07 (3)	0.44 \pm 0.00 (2)
Total solids (g/L)	–	6.34 \pm 0.08 (2)
Volatile solids (g/L)	–	4.54 \pm 0.28 (2)
Total suspended solids (g/L)	0.47 \pm 0.01 (3)	0.22 \pm 0.00 (2)
Volatile suspended solids (g/L)	0.34 \pm 0.02 (3)	0.02 \pm 0.00 (2)
Oil & fats (mg/L)	–	14.57 \pm 0.30 (2)
Volatile fatty acids (mg/L)	0.31 \pm 0.10 (3)	ND ^c

^a Measured in 25% OMW-1; ^b only one measurement due to limited sample volume; ^c ND: not detected

50 mL of OMW was added in sealed bottles of high-density polyethylene (HDPE) which contained 200 or 500 mg of adsorbent, respectively. The bottles were placed on a flat shaker inside a temperature-controlled chamber. Measurements of physicochemical parameters in undiluted OMW samples and adsorption tests were performed in duplicate ($n = 2$) or triplicate ($n = 3$) as reported in the tables and figures, and the average values along with standard deviation (SD) are given. In figures, SD is presented as error bars.

Prior to adsorption tests, the OMW samples were drawn through a filter paper (MN 615, Macherey-Nagel, Germany) in a Buchner funnel using a vacuum pump to exclude large suspended solids. The initial P and K concentrations (C_0) at each dilution ratio of OMW with DI were measured before the adsorption tests aiming at a more accurate estimation of P and K removal percentage (Table 2). As can be seen in Table 2, some measured C_0 values do not vary proportionally with each other based on the dilution ratios reported. These notable deviations can be attributed to the potential change of C_0 during the storage of diluted OMW-1 and OMW-2 samples in the fridge at AUA for a few weeks, combined with the fact that some experimental series (adsorption kinetics, pH effect or dilution tests) for each OMW sample did not take place at the same time. Supernatant samples were withdrawn at

Fig. 1 Samples of diluted **a** OMW-1 (12.5%) and **b** OMW-2 (50%); Ca(OH)₂-treated clinoptilolite before **(c)** and after **(d)** the OMW adsorption



specific time intervals during and at the end of the tests, centrifuged for 5 min at 4000 rpm, and then analyzed within a few hours for P and K.

The effect of contact time on P adsorption was studied in bottles of 100 mL capacity containing 500 mg of CaT-Z and 50 mL of 12.5% OMW-1, 25% OMW-1, or 50% OMW-2. These diluted samples correspond to 87.5/12.5, 75/25, and 50/50 dilution ratios with DI (V_{DI}/V_{OMW}), respectively (Table 2). In the kinetic tests with 12.5% and 25% OMW-1, the initial pH was slightly adjusted to 7.7 and 7.5, respectively (Table 2), whereas supernatant samples (50–100 μ L) were withdrawn with a micropipette at 1, 2, 4, 8 h and at 1, 2, 3, and 4 d. In the kinetic test with 50% OMW-2 (initial pH adjusted to 8.0), samples were collected at 1, 2, and 4 h and then at 1, 2, 3, 4, 8, 14, and 21 d. Adsorption kinetics of K were studied up to 4 and 8 d in the 25% OMW-1 and 50% OMW-2 solution, respectively, without sampling at 8 h. The total sampling volume did not exceed 2.3% of the initial working one.

The influence of the initial pH of OMW on P and K removal by CaT-Z was examined in 12.5% OMW-1 and 50%

OMW-2 for 4 d (Table 2). The initial pH was adjusted to the desired values (5, 6, 7, 8, and 9) by adding a few drops of 0.1–1 M HCl and/or NaOH in a working OMW volume of 100 mL. However, due to the buffering capacity of the 50% OMW-2 solution, the adjustment of the initial pH at 5, 6 and 7 was performed adding 0.2, 0.1, and 0.05 mL of 37% HCl with a micropipette. Finally, 200 mg CaT-Z were added in 20 mL of adjusted OMW. The final pH of each solution was measured after 4 d.

Adsorption tests at five different dilution ratios of OMW-1 and OMW-2 with DI were conducted for 4 d at a CaT-Z dosage of 500 mg/50 mL. This experimental series aimed at investigating the adsorption affinity of CaT-Z even at low concentrations of P and K, and at determining the adsorption mechanisms through the application of isotherm models. The dilutions of OMW-1 approximately consisted of 50%, 25%, 12.5%, 6.25%, and 3.125% solutions (Table 2), achieved by consecutive two-fold dilutions in a 100 mL graduated cylinder, namely diluting a 50% OMW-1 solution with an equal volume of DI (50/50). The dilutions of OMW-2 were 50%,

Table 2 Experimental conditions of batch adsorption tests with diluted OMW-1 and OMW-2 samples (contact time = 4 d, CaT-Z dosage = 10 g/L, $T = 25$ °C)

Variable	Sample	Dilution ratio (V_{DI}/V_{OMW})	%OMW ^a	C_0 (mg P/L)	C_0 (mg K/L)	pH
Contact time	OMW-1	87.5/12.5	12.5	5.44 ± 0.48**	–	7.7
Contact time	OMW-1	75/25	25	11.57 ± 0.47**	411.4 ± 10.3**	7.5
Initial pH	OMW-1	87.5/12.5	12.5	5.41 ± 0.09*	242.5 ± 0.0**	5–9
Dilution	OMW-1	50/50	50	19.00 ± 0.33*	737.5 ± 35.4*	8.0 ± 0.05
		75/25	25	11.42 ± 0.27*	382.5 ± 24.7*	
		87.5/12.5	12.5	6.21 ± 0.33*	200.0 ± 3.5*	
		93.75/6.25	6.25	2.42 ± 0.09*	94.4 ± 0.9*	
		96.875/3.125	3.125	1.21 ± 0.04*	36.3 ± 0.0*	
Contact time	OMW-2	50/50	50	26.07 ± 0.37**	931 ± 4.7**	8.0
Initial pH	OMW-2	50/50	50	25.38 ± 1.04**	789.5 ± 9.5**	5–9
Dilution	OMW-2	50/50	50	30.12 ± 1.12**	1041.1 ± 9.3**	8.2 ± 0.05
		75/25	25	13.62 ± 0.44**	517.7 ± 8.2**	
		90/10	10	5.63 ± 0.08**	210.7 ± 5.0**	
		93.75/6.25	6.25	3.56 ± 0.04**	129.3 ± 1.2**	
		95/5	5	2.58 ± 0.06**	98.1 ± 0.5**	

^a %OMW = $100 \times V_{OMW}/(V_{DI} + V_{OMW})$; * duplicate measurement; **triplicate measurement

25%, 10%, 6.25%, and 5% (Table 2). The initial pH of all dilution ratios was slightly adjusted around the value 8.0 for OMW-1 and 8.2 for OMW-2, wherever it was necessary due to the buffering capacity of OMW.

Finally, a series of five adsorption stages was performed in 50% OMW-2 applying fresh CaT-Z (10 g/L) at each stage (duration of each stage: 4 d) in order to determine the total (cumulative) removal (%) of P and K. After each stage, the treated 50% OMW-2 was filtered through filter paper (MN 615, Macherey-Nagel), before entering the next adsorption stage. The OMW-2 volumes used from the first to the fifth stage were 30, 25, 20, 10, and 5 mL, respectively.

The adsorption capacity of CaT-Z for P or K at equilibrium, q_e (mg/g) and the respective removal efficiency ($R\%$) were calculated according to the following equations:

$$q_e = (C_0 - C_e)V/m \quad (1)$$

$$R\% = 100 \times (C_0 - C_e)/C_0 \quad (2)$$

where C_0 and C_e are the initial and equilibrium P or K concentrations (mg/L), respectively, V is the OMW volume (L), and m is the adsorbent mass (g).

Batch desorption tests

The fractionation of adsorbed P on CaT-Z was investigated through a sequential extraction method of three steps (0.5 M NaHCO₃ at pH 8.5, 0.1 M NaOH and 0.5 M HCl) as described in previous publications (Han et al. 2016; Mitrogiannis et al. 2018). The desorption procedure was applied on the loaded CaT-Z samples, obtained from the dilution tests with 25% OMW-1 and 50% OMW-2, using a CaT-Z/eluent ratio of 200 mg/20 mL. Prior to each desorption step, the CaT-Z was washed twice with deionized water and dried overnight in an oven at 60 °C. A modified procedure (100 mg CaT-Z/10 mL eluent) was applied as well on the same loaded CaT-Z sample in 50% OMW-2, by conducting an ethanol extraction step prior to the above mentioned three steps.

The desorption efficiency D (%) and capacity q_{des} (mg P/g) of each eluent after centrifugation were estimated according to the following equations: D (%) = $100 \times (C_{des}/C_{ads})$ (3) and $q_{des} = C_{des} V/m$ (4), respectively; where $C_{ads} = (C_0 - C_e)$ and C_{des} are the P concentrations (mg/L) in the solid phase and in the desorption solution, respectively; V is the eluent volume (L) and m is the loaded CaT-Z mass (g). Specifically, for the sample of the loaded CaT-Z in 50% OMW-1, the desorption capacity of NH₄-N (mg N/g) was also calculated at each of the three desorption steps.

Analytical methods

Phosphate phosphorus (P) and ammonium nitrogen (N) concentrations in OMW, expressed as mg P/L and mg N/L, were

measured at AUA in a UV-vis spectrophotometer (Hach-Lange DR 2800) according to the ascorbic acid (4500-P E) and phenate (4500-NH₃ F) Standard Methods (APHA 1999), respectively. In order to measure P in the colored OMW, a blank was prepared for each OMW sample by adding only 5 N H₂SO₄ and ammonium molybdate, (NH₄)₆Mo₇O₂₄·4H₂O, solution (APHA 1999). The organic compounds, total solids, volatile solids, total suspended solids, and volatile suspended solids of OMW-1 and OMW-2 (Table 1) were determined at LBEET according to the methods reported in Zagklis et al. (Zagklis et al. 2015). Total organic carbon (TOC) on the spent CaT-Z samples was measured at LBEET using an SSM-5000A solid sample combustion unit (Shimadzu) allowing the separate determination of total carbon (TC) and inorganic carbon (IC). Potassium and sodium were measured at AUA by a flame photometer (BWB XP, UK). Total alkalinity (as mg CaCO₃/L) was determined by titration to the endpoint pH 4.5 according to the Standard Method 2320 B (APHA 1999). All the reagents employed for the determination of calibration curves were of analytical grade. A portable conductivity (Consort C931, Belgium) and pH meter (Metrohm 827, Swiss), calibrated once a week, were used for the determination of OMW electrical conductivity (EC) and pH, respectively. Characterization of NZ and CaT-Z was performed in the laboratories mentioned in our previous studies (Mitrogiannis et al. 2017; Mitrogiannis et al. 2018) by X-ray diffraction (XRD), scanning electron microscopy-energy dispersive system (SEM-EDS), and infrared attenuated total reflectance (IR-ATR).

In situ major element compositions were determined in polished mounted grains in resin using an electron probe micro-analyzer (EPMA) JEOL JXA-8900 Superprobe equipped with four wavelength-dispersive spectrometers (WDS) and one energy dispersive spectrometer (EDS) at the Laboratory of Mineralogy and Geology, AUA. All analyses used a 15-kV accelerating voltage, 15-nA beam 5 μm wide, 20 s on-peak counting time and 10 s for each background. Natural mineral standards used were quartz (Si), ilmenite (Ti), corundum (Al), fayalite (Fe), olivine (Mg, Ni), diopside (Ca), microcline (K), jadeite (Na), apatite (P), and chromite (Cr). Further, X-ray maps were collected from selected areas using the JEOL JXA-8900 Superprobe at 15 kV, 50 nA, 0.5-μm step size, and 100-ms dwell time giving collection times between 2 and 5 h.

Results and discussion

Comparison of NZ and CaT-Z adsorption performances for P

A comparative P adsorption test was performed for 4 d in triplicate using NZ and CaT-Z in a 25% OMW-1 solution

which contained 12.95 mg P/L. The test revealed for NZ an adsorption capacity of 0.13 ± 0.06 mg P/g and a removal efficiency of $10.1 \pm 4.9\%$. These values were lower than those of CaT-Z which adsorbed 0.96 ± 0.02 mg P/g and removed $73.9 \pm 1.7\%$ of P. The comparative test was performed without pH adjustment of 25% OMW-1 sample. Our previous adsorption study with real fresh urine has shown the higher P adsorption capacity of CaT-Z than that of NZ, as a result of the enhanced point of zero charge of CaT-Z surface ($\text{pH}_{\text{pzc}} = 9.90$) after the pretreatment of NZ with $\text{Ca}(\text{OH})_2$ (Mitrogiannis et al. 2018). Recent studies have also reported the phosphate recovery from real wastewater by raw clinoptilolite (NZ) which has no anion exchange capacity. However, they relate these findings to the concentration of coexisting solute $\text{NH}_4\text{-N}$ and its adsorption on NZ as well as to P precipitation in the liquid phase (Lin et al. 2014; Wan et al. 2017). Based on the above comparative results for P removal, further experiments were conducted using only CaT-Z.

Effect of contact time on P and K removal from OMW-1 and OMW-2

The experimental kinetic curves show that P concentration in 12.5% OMW-1, 25% OMW-1, and 50% OMW-2 decreased faster in the first 24–48 h of contact with CaT-Z and then at a slower rate up to 4 d, approaching an equilibrium (Fig. 2a). In the first 24 h, 40.8% and 48.0% of P was removed from the 12.5% and 25% OMW-1 solutions, respectively. After 4 d, the respective $R\%$ was 56.7% and 75.9%. In 50% OMW-2, most of the P (64.8%) was removed by CaT-Z within 24 h, whereas equilibrium was reached within 4–8 d. The observed $R\%$ and q_t values were in the range of 73.6–75.3% and 1.92–1.96 mg P/g, respectively. On the other hand, the equilibrium of K removal from 25% OMW-1 and 50% OMW-2 was achieved faster than that of P, namely within 24 h, exhibiting a $R\%$ of 27.2% and 20.7% as well as q_t values of 11.2 and 19.3 mg K/g, respectively (Fig. 2b). In the first 24 h, the concentration of K reduced to 299.3 mg/L in 25% OMW-1 and to 738.0 mg/L in 50% OMW-2. The simultaneous removal of P and K by CaT-Z has been earlier observed in aqueous solution containing KH_2PO_4 reagent (Mitrogiannis et al. 2017). In the present study, the faster removal kinetics of K than that of P may be attributed either to the higher initial concentration of K in both OMW samples (Table 2), resulting in a higher driving force for the diffusion of K into the porous CaT-Z, or to the presence of more accessible binding sites (functional groups) for K at the external and internal CaT-Z surface (Malamis and Katsou 2013). Another reason can be the different, dominant adsorption mechanism of K (cation exchange) than that of P (ligand exchange, surface precipitation) (see Sections 3.7.2 and 3.7.3). For both cations and anions, the ion exchange mechanism (outer-sphere complexation) is faster than the inner-sphere complexation (ligand exchange) and surface

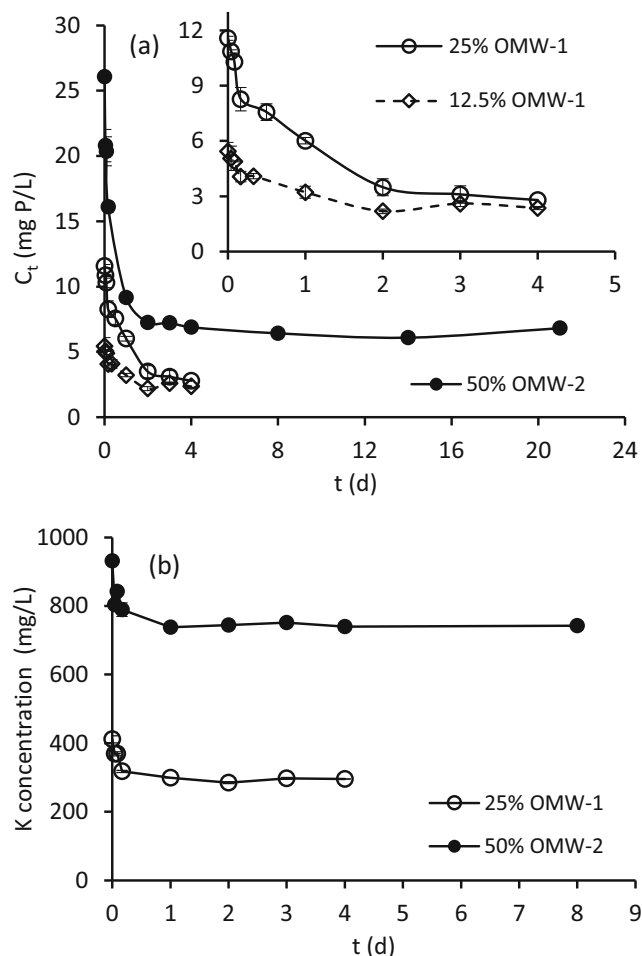


Fig. 2 a Variation of P concentration with time in 12.5% OMW-1 ($n = 3$) (inset), 25% OMW-1 ($n = 2$) (inset), and 50% OMW-2 ($n = 3$) contacted with CaT-Z; b variation of K concentration with time in 25% OMW-1 ($n = 2$) and 50% OMW-2 ($n = 3$) contacted with CaT-Z (CaT-Z dosage = 500 mg/50 mL, $T = 25^\circ\text{C}$). Numbers (n) in parentheses refer to replicates of the tests

precipitation (Loganathan et al. 2014; Malamis and Katsou 2013). It is also known that the adsorption and ion exchange rate in porous solids is constrained by mass transfer resistances (diffusion-controlled processes) into the pore structure rather than by chemical reaction kinetics (Inglezakis et al. 2019). Thus, chemical reaction of P and K with the internal sites of CaT-Z pore walls does occur; however, diffusion limitations decrease the reaction rate (Makris et al. 2004).

Effect of OMW-1 and OMW-2 pH on P and K removal

The change of initial pH of 12.5% OMW-1 from 6 to 9 slightly affected the removal percentage of P by CaT-Z which ranged from 61.9% to 67.2% (Fig. 3a). The lowest and highest $R\%$ of P were observed at pH 5 (54.7%) and 7 (67.2%), respectively, corresponding to a q_e of 0.30 and 0.36 mg P/g. The final pH of the 12.5% OMW-1 solutions with initial values 5–8 increased,

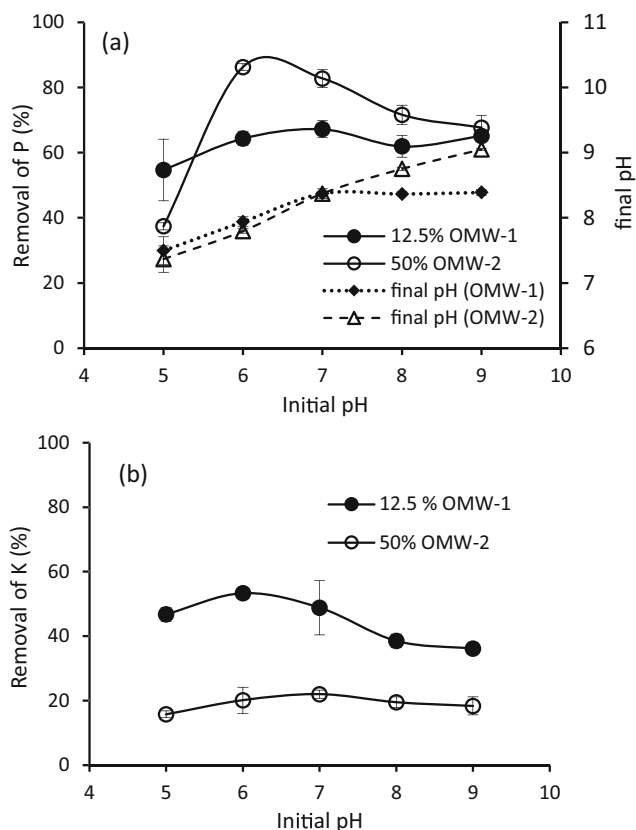


Fig. 3 Effect of initial pH of 12.5% OMW-1 and 50% OMW-2 solutions on **a** P and **b** K removal efficiency by CaT-Z (CaT-Z dosage = 200 mg/20 mL, contact time = 4 d, $T = 25\text{ }^{\circ}\text{C}$, $C_0 = 5.41\text{ mg P/L}$ and 242.5 mg K/L in 12.5% OMW-1; $C_0 = 25.38\text{ mg P/L}$ and 789.5 mg K/L in 50% OMW-2). The adsorption tests were performed in triplicate

ranging from 7.50 to 8.37, whereas it showed similar values (8.37–8.39) in the solutions with initial pH 7–9 (Fig. 3a).

A different behaviour of P removal by CaT-Z was observed with the variation of initial pH in the 50% OMW-2 solution. The highest $R\%$ occurred at pH 6 ($R\% = 86.2\%$ and $q_e = 2.19\text{ mg P/g}$) whereas $R\%$ decreased in the pH range of 7–9 ($R\% = 67.7\%$ and $q_e = 1.72\text{ mg P/g}$ at pH 9) (Fig. 3a). These results might be related to a stronger negative influence of OMW organic matter and alkalinity on P adsorption occurring in the less diluted OMW-2 (50%) than in the more diluted 12.5% OMW-1. It is known that an excess alkalinity is produced during anaerobic digestion processes (Dareioti et al. 2009; Lin et al. 2014), and that carbonate/bicarbonate anions inhibit the inner-sphere complexation (via ligand exchange) of various calcium phosphate (Ca-P) phases on the CaT-Z surface (Lin et al. 2014; Mitrogiannis et al. 2018). The final pH of the 50% OMW-2 solutions after adsorption steadily increased in the range of 7.37–9.05 with increasing initial pH from 5 to 9 (Fig. 3a).

Regarding the $R\%$ of K^+ from 12.5% OMW-1 (Fig. 3b), it increased from 46.7 to 53.3% (12.9 mg K/g) between the pH 5 and 6, but then decreased from 48.8% at pH 7 to 36.1%

(8.8 mg K/g) upon increasing the initial pH to 9. On the other hand, the $R\%$ of K from 50% OMW-2 ranged from 15.8 to 22.0% (Fig. 3b) and, as expected, was lower than that in 12.5% OMW-1 due to the higher initial K concentration in 50% OMW-2 (Malamis and Katsou 2013). The removal of K from 50% OMW-2 increased from 15.8% at pH 5 to 22.0% at pH 7, whereas it decreased to 18.3% at pH 9.

Effect of OMW-1 and OMW-2 dilution

Removal of P at different dilution ratios of OMW-1 and OMW-2

The removal efficiency ($R\%$) of P by CaT-Z ranged from 19.0 to 70.4% in OMW-1 and from 69.3 to 85.9% in OMW-2 (Fig. S1a). It should be noted that $R\%$ values for P do not present a monotonic increasing trend with decreasing initial P concentrations, generated from higher OMW-1 and OMW-2 dilutions, as usually occurs during adsorption processes (Malamis and Katsou 2013; Mitrogiannis et al. 2017; Mitrogiannis et al. 2018). Unknown mechanisms of unfavorable and antagonistic adsorption related to the complex chemical composition of OMW-1 and OMW-2 (Table 1) should be responsible for the lower affinity of P by CaT-Z at higher dilution ratios (specifically at 3.125–6.25% OMW-1 and 5% OMW-2 solutions) and for the discrepancies in the equilibrium data (Fig. S1a).

The experimental data at various dilution ratios of OMW-1 and OMW-2 with DI were fitted to isotherm models (Table 3). The model parameters were calculated via the method of the non-linear optimization, minimizing the error function of residual sum of squares (RSS) (Table 3). For the minimization, the generalized reduced gradient algorithm (GRGS) of the Microsoft Excel Solver tool was used. The fitting quality of each isotherm model was also evaluated by the coefficient of determination (R^2) between the experimental and model predicted q_e values. The P adsorption from diluted OMW-1 on CaT-Z exhibited a sigmoidal isotherm (S-shaped) (Fig. 4a) which was successfully interpreted by the theoretical model of Zhu and Gu based on the two-step adsorption mechanism and the mass action treatment (Zhu and Gu 1989; Zhu and Gu 1991). The value of the aggregation number $n (> 1)$ (Table 3) suggests the formation of surface aggregates (so-called hemimicelles) on the second adsorption step (Zhu and Gu 1991). The Type-V (S-shaped) isotherms present one inflection point where the curve concavity changes (Inglezakis et al. 2018). At this point, namely at a specific C_e , the unfavorable equilibrium and antagonistic effects of coexisting solutes, like hydrophobic OMW organics (Blika et al. 2009), are overcome and a cooperative adsorption occurs (Inglezakis et al. 2018). A sigmoidal isotherm was also observed for P adsorption from anaerobically digested cattle wastewater on $\text{Ca}(\text{OH})_2$ treated bentonite (Markou et al. 2018).

Table 3 Parameters of isotherm models for P and K adsorption from OMW-1 and OMW-2 onto CaT-Z (CaT-Z dosage = 10 g/L, contact time = 4 d, $T = 25\text{ }^{\circ}\text{C}$)

Model	Equation	Parameter	OMW-1 PO ₄ -P	OMW-1 K ⁺	OMW-2 PO ₄ -P	OMW-2 K ⁺
Zhu and Gu ^a	$q_e = \frac{q_m k_1 C_e (\frac{1}{n} + k_2 C_e^{n-1})}{1 + k_1 C_e (1 + k_2 C_e^{n-1})}$	$q_{e,\text{exp}}$ (mg/g)*	1.08	12.8	2.14	15.8
		k_1 ((L/mg) ^{1/n})	5.13×10^{-3}	–	–	–
		k_2 ((L/mg) ^{1/n})	0.250	–	–	–
		n	6.42	–	–	–
		RSS ^d	0.0049	–	–	–
		R^2	0.994	–	–	–
Langmuir ^b	$q_e = \frac{q_{\text{max}} K_L C_e}{1 + K_L C_e}$	q_{max} (mg/g)	–	15.5	4.44	17.3
		K_L (L/mg)	–	0.0073	0.1060	0.0124
		R_L	–	0.16–0.79	0.24–0.79	0.07–0.45
		RSS	–	0.223	0.0464	0.631
		R^2	–	0.998	0.982	0.992
		R^2	–	0.998	0.982	0.992
Freundlich ^c	$q_e = K_F C_e^{1/n}$	K_F (mg/g)/(mg/L) ^{1/n}	–	0.80	0.44	2.38
		n	–	2.27	1.37	3.49
		RSS	–	3.685	0.0590	6.4543
		R^2	–	0.956	0.978	0.918
		R^2	–	0.956	0.978	0.918
		R^2	–	0.956	0.978	0.918

*For C_0 corresponding to 50% OMW-1 and OMW-2

^a Zhu and Gu [37]: q_m is the maximum experimental q_e (1.084 mg/g), k_1 and k_2 are the equilibrium constants of the first and second adsorption step, respectively; n is the aggregation number of surface hydrophobic aggregates ($n > 1$ for hemimicellization and $0 < n < 1$ for multi-site adsorption)

^b Langmuir: q_{max} (mg/g) is the theoretical maximum monolayer adsorption capacity and b (L/mg) is the Langmuir constant related to the affinity and binding energy; $R_L = 1/(1 + (b C_0))$ is the dimensionless separation factor

^c Freundlich: K_F [(mg/g)/(mg/L)^{1/n}] is the Freundlich isotherm constant representing the adsorption capacity and n is a dimensionless factor related to the adsorption intensity and surface heterogeneity

^d $\text{RSS} = \sum_{i=1}^n (q_{e,\text{exp}} - q_{e,\text{cal}})^2$ is the residual sum of squares containing the experimental and model predicted values of q_e , respectively, and n is the number of experimental points

The experimental data of OMW-2 were well fitted to both the Langmuir and Freundlich isotherms (Fig. 4a), suggesting a complex P adsorption mechanism. Langmuir equation exhibited a slightly better fit than Freundlich due to the lower RSS and higher R^2 value (Table 3), although the experimental q_e values do not present a typical plateau. The theoretical assumption of the Langmuir model for adsorption on homogeneous surfaces does not agree with the surface heterogeneity of CaT-Z before adsorption (Mitrogiannis et al. 2017, Mitrogiannis et al. 2018). However, it could be related either to P adsorption on a finite number of binding sites containing Ca²⁺ ions (Mitrogiannis et al. 2017) or to a less heterogeneous CaT-Z surface after adsorption due to its coverage with OMW organic matter (Fig. 1d).

Removal of K at different dilution ratios of OMW-1 and OMW-2

The treatment of diluted OMW-1 and OMW-2 with CaT-Z decreased the concentration of K by 17.3–46.1% and 15.1–57.7%, respectively (Fig. S1b). The K removal efficiency

($R\%$) positively correlated with the increasing dilution of both OMW samples, namely with decreasing initial K concentration (Table 2). The relationship of CaT-Z adsorption capacity at equilibrium with the residual K concentration at five different dilution ratios of OMW-1 and OMW-2 is presented in Fig. 4b. In both OMW samples, the equilibrium data are best described by the Langmuir isotherm ($R^2 \geq 0.992$ and $\text{RSS} \leq 0.631$) and the values of the factor R_L ($0 < R_L < 1$) indicate a favorable adsorption process (Table 3). The same model has been reported to describe very well the K adsorption from seawater reverse osmosis brine onto clinoptilolite (Naidu et al. 2018). The higher adsorption capacities for P and K in OMW-2 than in OMW-1 (Fig. 4), are due to the higher initial concentrations of both solute ions in the studied dilution ratios of OMW-2 than in these of OMW-1 (Table 2).

Removal of NH₄-N from diluted OMW-1 and OMW-2

As shown in Table 1, both undiluted OMW samples contained similar NH₄-N amounts, which were lower and very minor than those of P and K, respectively. Consequently, our work

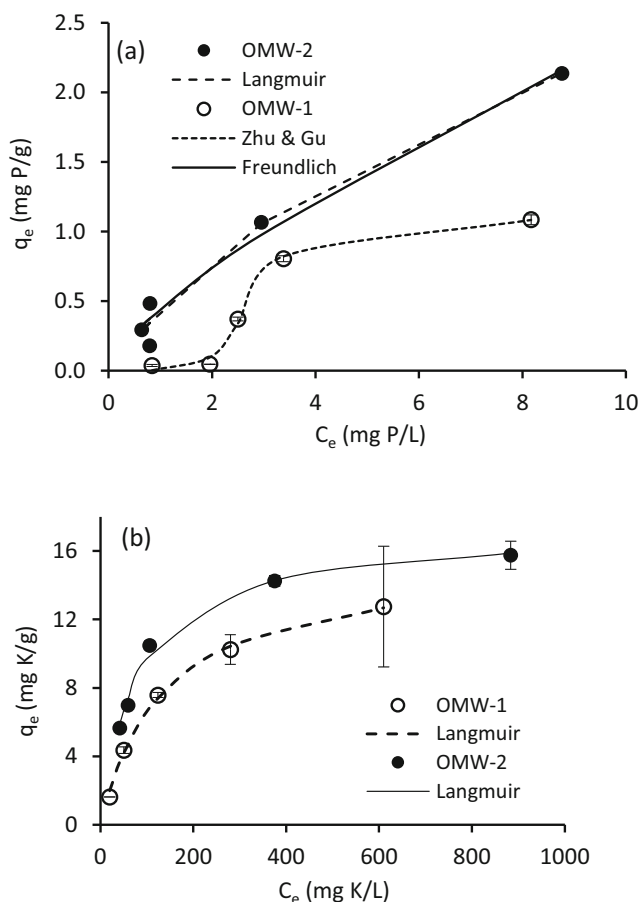


Fig. 4 Experimental equilibrium data of P (a) and K (b) adsorption from OMW-1 and OMW-2 at different dilution ratios (CaT-Z dosage = 500 mg/50 mL, contact time = 4 d, T = 25 °C; the curves represent the best-fitted isotherm models). The tests were performed in triplicate

focused on P and K recovery; however, the residual $\text{NH}_4\text{-N}$ concentrations after adsorption was measured in the 25% OMW-1, 25% OMW-2, and 50% OMW-2 solutions. After 96 h of contact with CaT-Z, the $\text{NH}_4\text{-N}$ concentration decreased from 4.01 ± 0.10 to 3.37 ± 0.13 mg/L in 25% OMW-1, from 4.65 ± 0.08 to 3.07 ± 0.12 mg/L in 25% OMW-2, and from 10.76 ± 0.30 to 8.69 ± 0.23 mg/L in 50% OMW-2. These changes correspond to $R\%$ of $15.97 \pm 3.33\%$, $33.89 \pm 2.49\%$, and $19.26 \pm 2.15\%$, as well as to adsorption capacities of 0.06 ± 0.01 , 0.16 ± 0.01 and 0.21 ± 0.02 mg N/g, respectively. To sum up the results of the sections “Removal of P at different dilution ratios of OMW-1 and OMW-2,” “Removal of K at different dilution ratios of OMW-1 and OMW-2,” and “Removal of $\text{NH}_4\text{-N}$ from diluted OMW-1 and OMW-2,” CaT-Z showed low removal efficiencies for P, K, and $\text{NH}_4\text{-N}$ in less diluted OMW samples (50%) and at the given CaT-Z dosage (10 g/L). So, further tests are needed using higher CaT-Z dosages in order to increase the $R\%$ of nutrients from undiluted OMW and to make the treatment process more feasible in full-scale applications.

Chemical extraction of adsorbed P

The sequential desorption of adsorbed P from the loaded CaT-Z in 25% OMW-1 and 50% OMW-2 revealed that the loosely bound and plant-available P (denoted as LB-P or $\text{NaHCO}_3\text{-P}$) constituted the major P fraction (Guaya et al. 2016; Yang et al. 2015). The desorption efficiency ($D\%$) of the first step was 77.4% and 73.8% for the OMW-1 and OMW-2 loaded adsorbent, respectively (Fig. 5). The respective desorption capacity (q_{des}) was 0.56 and 1.45 mg P/g CaT-Z. The LB-P was also found to be the dominant fraction on CaT-Z contacted with diluted real fresh urine characterized by similar initial P concentrations (Mitrogiannis et al. 2018). The contribution of aluminum (hydro)oxides bound P (Al-P or NaOH-P) and calcium associated P (Ca-P or HCl-P) (Guaya et al. 2016; Han et al. 2016) on the total $D\%$ was found to be very minor for both the 25% OMW-1 (9.2% Al-P and 9.4% Ca-P) and the 50% OMW-2 loaded CaT-Z (2.0% Al-P and 7.4% Ca-P). The total $D\%$ of the three extraction steps was estimated at 95.9% and 83.2% of the total removed P from 25% OMW-1 and 50% OMW-2, respectively, and the total q_{des} amounted to 0.69 and 1.64 mg P/g. A similar value of q_{des} (2.13 ± 0.07 mg P/g) was found for CaT-Z after contact with 5% fresh urine solution containing 29.4 ± 0.4 mg P/L (Mitrogiannis et al. 2018). The total $D\%$ values also suggest a minor removal of P due to washing of CaT-Z with deionized water after the adsorption process (water-soluble P) or due to precipitation in the liquid phase (Mitrogiannis et al. 2018). This possibility is not often taken into account in adsorption studies with real and high-strength wastewater leading to an overestimation of the q_e values. Simultaneously, the presence of adsorbed $\text{NH}_4\text{-N}$ on CaT-Z after being contacted with 50% OMW-2 was confirmed by a low total q_{des} of 0.144 mg N/g obtained from the first (0.077 mg/g) and the second (0.067 mg/g) desorption

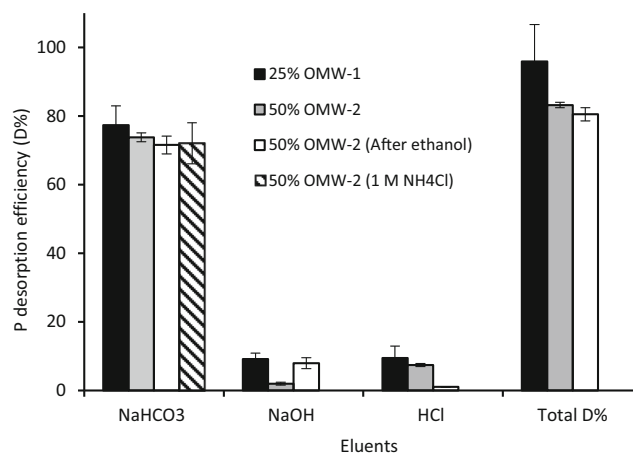


Fig. 5 Sequential desorption of P from the loaded CaT-Z in 25% OMW-1 and 50% OMW-2. The NH_4Cl eluent was applied only to the loaded CaT-Z in 50% OMW-2 (OMW-1: $C_0 = 11.42 \pm 0.27$ mg/L; OMW-2: $C_0 = 30.12 \pm 1.12$ mg/L, CaT-Z/eluent ratio = 10 g/L, contact time of each step = 24 h, T = 25 °C). The desorption tests were performed in triplicate

step. The magnitude of q_{des} is in accordance with the q_e of 0.21 mg N/g mentioned in the previous section (3.4.3.).

Raw or acidified ethanol is widely used as a bio-compatible desorbing eluent for the recovery of polyphenols from various adsorbents loaded with OMWs (Frasconi et al. 2016; Scoma et al. 2011; Zagklis et al. 2015). The ethanol application to the above mentioned sample of 50% OMW-2 loaded CaT-Z, prior to the three-step extraction procedure, did not significantly affect either the P desorption efficiency of the LB-P fraction (71.6%) or the total $D\%$ (80.5%) (Fig. 5). This finding suggests that CaT-Z could be used in an integrated OMW treatment process aiming at the recovery of various added-value compounds such as polyphenols and inorganic nutrients. Finally, the one-step extraction of P by 1 M NH_4Cl revealed a similar desorption efficiency of LB-P (72.1%) (Yang et al. 2015) (Fig. 5) and generated a desorbing solution for potential plant fertilization containing both N and P.

Sequential treatment of OMW-2 with fresh CaT-Z

The sequential treatment of 50% OMW-2 with fresh CaT-Z at each step resulted in total removal of 87.5% for P and 74.9% for K after the fifth adsorption stage (total duration of 20 d). The residual concentrations at the end of the process were found to be 3.76 mg P/L and 261.1 mg K/L (Fig. 6a, b). However, the removal performance ($R\%$) of fresh CaT-Z for P exhibited a downward trend from step to step whereas the $R\%$ for K showed an increasing linear trend ($R^2 = 0.981$) (Fig. 6b). The $R\%$ for P decreased from 65.3% in the first step to 11.1% in the fifth one (Fig. 6a). This decreasing $R\%$ may reflect the hindering and competing influence of OMW compounds such as carbonates and anionic organics (phenols) which reduced the available binding sites for P. Carbonates strongly compete with phosphates for complexation with surface Ca^{2+} ions (Lin et al. 2014; Mitrogiannis et al. 2017). The sequential adsorption treatment could be performed in basket batch reactors, where the granular adsorbent particles are fixed in sieve-like baskets (Worch 2012). After each OMW treatment stage, the spent CaT-Z particles can be replaced with new ones, increasing however the total amount of used adsorbent and the operational treatment costs.

Adsorbent characterization and nutrients removal mechanisms

XRD analysis

The XRD patterns of raw NZ and CaT-Z before adsorption have been described in a previous work (Mitrogiannis et al. 2018). The samples of CaT-Z examined after adsorption in 50% OMW-1 and OMW-2 solutions did not reveal changes in their mineral modes. The phases of clinoptilolite, quartz, illite, anorthite (plagioclase), microcline (K-feldspar),

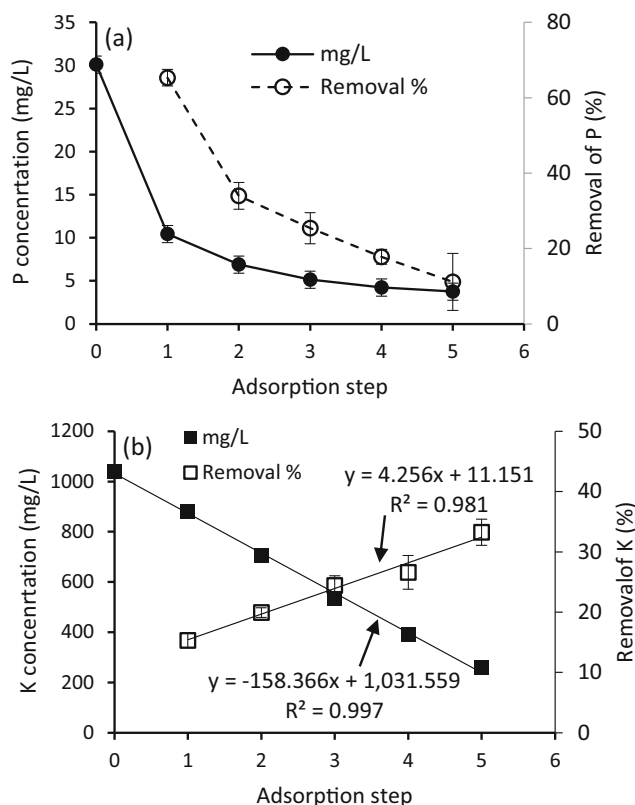


Fig. 6 Effect of a five-step sequential treatment of 50% OMW-2 with fresh CaT-Z on P and K removal ($C_0 = 30.12 \pm 1.12$ mg P/L and 1041.1 ± 9.3 mg K/L, CaT-Z dosage = 10 g/L, contact time of each step = 4 d, $T = 25$ °C). The adsorption tests were performed in triplicate

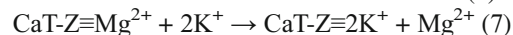
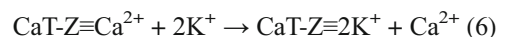
vermiculite and montmorillonite were detected in the XRD patterns (Fig. S2a and b). On the other hand, no newly formed K or P bearing mineral phases were detected suggesting adsorption either as an amorphous phase or at a modal content below the detection limit of the XRD technique.

SEM-EDS, X-ray maps, and EPMA analyses

The SEM images of CaT-Z contacted with 50% OMW-1 and 50% OMW-2 displayed a smoother surface (Fig. S3b and c) compared to the rough one before adsorption (Mitrogiannis et al. 2017). As shown in Fig. 1d, CaT-Z surface was brown-colored after adsorption. The organic nature of this layer is confirmed by the measured TOC values of CaT-Z samples contacted with 50% OMW-1 and OMW-2, amounted to 0.37 ± 0.03 and 1.47 ± 0.03 mg TOC/g, respectively. In contrast, no TOC was detected in NZ and CaT-Z before adsorption. The lower content of TOC per g of CaT-Z contacted with 50% OMW-1 than with 50% OMW-2 is in contradiction with the higher content of dissolved organics in OMW-1 than in OMW-2 (Table 1). However, both values of mg TOC/g are significant compared to the respective q_e for P, namely 1.08 ± 0.04 and 2.14 ± 0.02 mg P/g in 50% OMW-1 and OMW-2, respectively (Table 3). Furthermore, Ca- and P-rich crystals

were observed on the surface of CaT-Z contacted with 25% OMW-1 (Fig. S3a, EDS spectrum #1), whereas the co-presence of Ca and P was also detected by the single-point elemental analysis of CaT-Z contacted with 50% OMW-1 and OMW-2 (Fig. S3b and c, spectra #2 and #3).

Prior to the individual compositional analyses, a detailed X-ray mapping of various elements was performed in order to evaluate the degree, quality, and distribution of the adsorbed elements on the CaT-Z surface. Representative grains (Fig. 7) were first scanned using the back-scattered electrons (BSE) and then mapped for Al, K, Ca, and P (Fig. 8). The X-ray maps for the selected elements revealed the co-occurrence of Ca and P and the presence of K at the matrix. In particular, Ca and P show a heterogeneous distribution and adsorption in the zeolitic matrix between the silicate clasts (e.g., quartz and feldspar) (Fig. 8). The absence of P₂O₅ in CaT-Z before adsorption as well as the P₂O₅ content of 0.01–0.05 wt% in the loaded CaT-Z (Table 4) confirmed the P adsorption on the solid phase. Similarly, potassium (K) was incorporated in such areas, where the altered silicates lead to a smooth (or at least non-rough under the resolution of EPMA) surface of the zeolitic matrix (Fig. 7c, d, and Fig. 8). The compositional data of the loaded CaT-Z derived from EPMA analysis showed an increase of K₂O and Na₂O content which were adsorbed in the range of 6.97–9.37 wt% and 0.10–0.40 wt%, respectively (see single-point analyses #4–13 in Table 4). These findings were accompanied by a decrease of CaO (0.78–1.20 wt%) and MgO (0.54–0.88 wt%) percentage compared with that before adsorption (analyses #1–3, Table 4), indicating an ion exchange mechanism. The cation exchange between solute K⁺ ions and bivalent cations of CaT-Z surface (≡) can be described by the following equations:



IR-ATR analysis

The assignment of the bands observed in the IR-ATR spectra of the NZ and CaT-Z before the adsorption (Fig. 9) is given in our earlier work (Mitrogiannis et al. 2017). The IR spectrum of NZ contacted with 50% OMW-2 is similar to the pristine NZ, the main differences being the slight downshift of the strongest band to 1012 cm⁻¹ and the appearance of a low-frequency 780-cm⁻¹ shoulder in the 790-cm⁻¹ band for the OMW-2 loaded sample.

The IR spectra of the CaT-Z contacted with 50% OMW-1 and OMW-2 bear similarities with the pristine CaT-Z (Fig. 9). The most important differences are the relative intensity changes of the bands attributed to aragonite and calcite: (a) In the 50% OMW-1 loaded CaT-Z, the 858 and 1475 cm⁻¹ bands, assigned to the aragonite ν₂ and ν₃ CO₃²⁻ anion modes, respectively, show a reduced relative intensity with respect to the corresponding calcite modes observed respectively at 875 and 1430 cm⁻¹ in this sample - this aragonite phase diminution is to be contrasted with the case of pristine CaT-Z, where aragonite is the majority phase; (b) in the 50% OMW-2 loaded CaT-Z sample, the ν₂ aragonite band disappears, leaving only the ν₂ calcite one with increased relative intensity, while the ν₃ broad envelope center downshifts from ca. 1475 to 1438 cm⁻¹; (c) at the same time, the 1018-cm⁻¹ composite band downshifts to ca. 1011 cm⁻¹ and the shoulder at 780 cm⁻¹ appears again only for the 50% OMW-1 loaded CaT-Z sample, as in the case of the 50% OMW-2 loaded NZ.

One way to account for the retention of the carbonate bands in both OMW loaded CaT-Z samples is to assume an ion exchange mechanism operating between the Ca²⁺ and K⁺ ions. We note that the vibrational mode shape and frequency

Fig. 7 Polished, mounted on resin, grains of CaT-Z contacted with 50% OMW-2 (a, c). Rectangles featured as panels “B” (a) and “D” (c) are presented as enlarged parts of small grains (b, d).

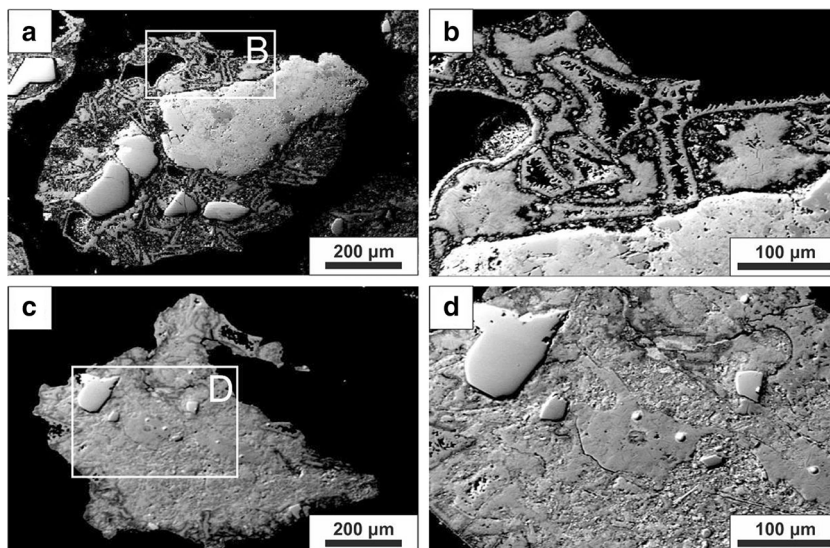
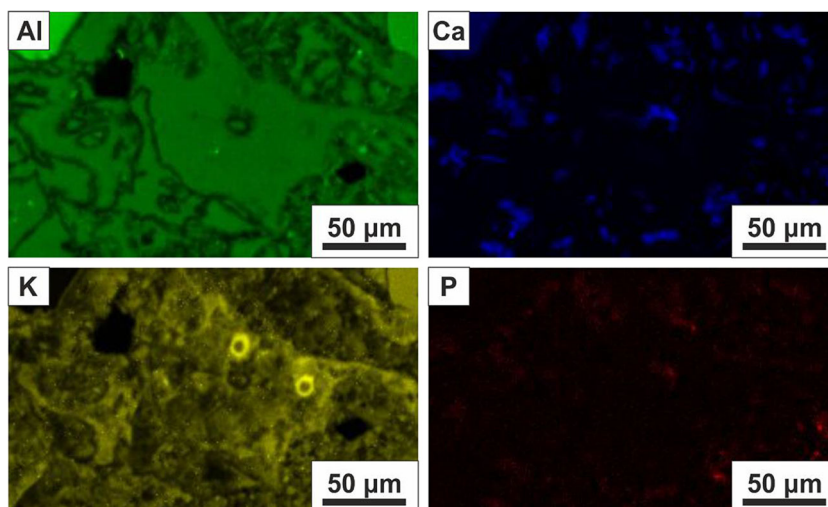


Fig. 8 Panels of qualitative X-ray maps (Al, Ca, K, P) of the clinoptilolite-rich area featured in Fig. 7c, d. Brighter color-scale values in the X-ray maps indicate a higher concentration of the indicated elements. The two bright spots shown in the K X-ray map correspond to surface damage due to electron beam after individual analyses



of the carbonate anion infrared bands depend on deviations from the trigonal symmetry and the type of the charge-balancing cation: (a) ν_3 is a doubly degenerate CO_3^{2-} mode which is seen to split in our case, as a result of the perturbation of the carbonate anion D_{3h} trigonal symmetry in both the

aragonite and calcite phases (Kamitsos et al. 1989). This is why the $\nu_3 \text{CO}_3^{2-}$ asymmetric stretch mode is seen as such a broad envelope ($1400\text{--}1550 \text{ cm}^{-1}$ in pristine CaT-Z) (Mitrogiannis et al. 2017); (b) an additional reason for the observation of these broad envelopes, is the fact that in the

Table 4 EPMA compositional data (expressed as oxides in wt%) of CaT-Z before (1–3) and after adsorption (4–13) in 50% OMW-2

CaT-Z sample	Before adsorption			After adsorption									
	1	2	3	4	5	6	7	8	9	10	11	12	13
Analysis ^a													
SiO ₂	64.8	69.7	68.0	67.5	70.4	67.2	65.5	66.5	67.3	66.9	66.2	65.8	65.9
Al ₂ O ₃	13.0	12.4	12.2	12.2	12.6	11.6	12.3	12.1	11.4	12.1	12.3	12.2	11.9
FeO _{tot}	0.11	0.03	0.01	0.07	0.06	0.04	0.06	0.02	0.02	0.02	0.09	0.02	0.02
MgO	0.92	0.99	0.98	0.62	0.72	0.75	0.82	0.658	0.54	0.68	0.70	0.78	0.68
CaO	2.55	2.83	2.26	1.20	1.16	0.98	1.08	0.945	0.78	0.81	0.90	0.98	1.04
Na ₂ O	0.04	0.04	0.04	0.33	0.40	0.15	0.10	0.143	0.11	0.13	0.14	0.14	0.24
P ₂ O ₅	bdl ^b	bdl	bdl	0.01	0.05	0.04	bdl	0.02	0.02	bdl	bdl	0.01	0.02
K ₂ O	1.49	2.07	2.26	7.80	6.98	7.59	7.74	9.15	7.90	9.32	9.37	8.20	7.14
Total	82.9	88.1	85.7	89.7	92.4	88.4	87.7	89.5	88.1	90.0	89.8	88.2	87.0
Calculated for 36 oxygens													
Si ⁴⁺	14.786	15.006	15.024	14.959	14.897	14.920	14.718	14.747	14.993	14.761	14.672	14.741	14.850
Al ³⁺	3.496	3.146	3.177	2.935	3.146	3.041	3.259	3.156	2.997	3.145	3.224	3.213	3.161
Fe ⁺²	0.021	0.005	0.002	0.013	0.010	0.007	0.011	0.003	0.005	0.004	0.017	0.004	0.003
Mg ²⁺	0.313	0.318	0.323	0.206	0.228	0.248	0.275	0.218	0.180	0.224	0.232	0.260	0.228
Ca ²⁺	0.623	0.653	0.535	0.284	0.263	0.233	0.259	0.225	0.186	0.191	0.214	0.235	0.250
Na ⁺	0.018	0.017	0.017	0.143	0.165	0.065	0.043	0.062	0.048	0.059	0.061	0.061	0.103
P ⁵⁺	bdl	bdl	bdl	0.002	0.008	0.006	0.001	0.003	0.003	0.001	bdl	0.002	0.004
K ⁺	0.434	0.569	0.637	2.207	1.882	2.153	2.216	2.590	2.249	2.623	2.651	2.342	2.053
Si ⁴⁺ +Al ³⁺	18.282	18.152	18.201	17.894	18.024	17.962	17.977	17.903	17.990	17.906	17.897	17.953	18.011
Si ⁴⁺ /(Al ³⁺ +Fe ²⁺)	4.204	4.761	4.727	5.110	4.740	4.913	4.528	4.676	5.008	4.699	4.567	4.592	4.701
Si ⁴⁺ /(Si ⁴⁺ +Al ³⁺ +Fe ²⁺)	0.808	0.826	0.825	0.835	0.825	0.830	0.818	0.824	0.833	0.824	0.819	0.821	0.824

^a Numbers in parentheses correspond to probe locations given in Fig. 7; ^b *bdl*: below detection limit

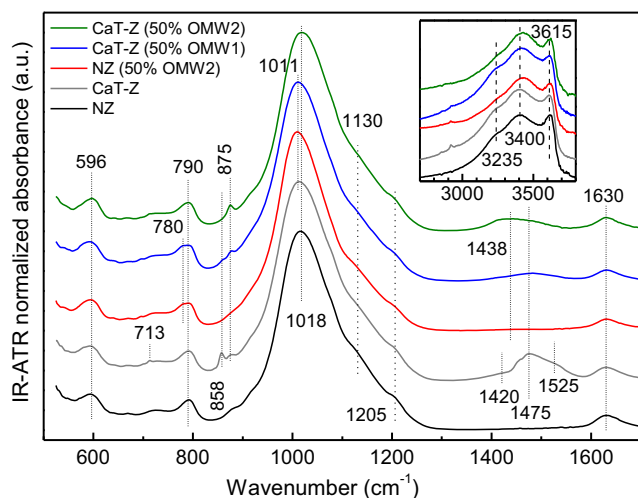


Fig. 9 IR-ATR spectra of the NZ (black line), CaT-Z (gray line), NZ contacted with 50% OMW-2 (red line), CaT-Z contacted with 50% OMW-1 (blue line), and CaT-Z contacted with 50% OMW-2 (green line). For the inset, the spectra were normalized with respect to the water H–O–H bending vibration intensity at 1630 cm^{-1}

case of K_2CO_3 the unperturbed ν_2 and ν_3 CO_3^{2-} modes are observed at 880 cm^{-1} and 1400 cm^{-1} respectively (Hopkinson et al. 2018).

Thus, the presence of potassium would seem to favor the stabilization of calcite-type K_2CO_3 especially in the 50% OMW-2 loaded CaT-Z sample. The 1350–1500 cm^{-1} envelope centered at ca. 1438 cm^{-1} in 50% OMW-2 loaded CaT-Z can be understood as a convolution of the CaCO_3 and K_2CO_3 calcite ν_3 CO_3^{2-} modes. A much weaker broadening effect of the same origin would be expected for the ν_2 mode (875 cm^{-1} for CaCO_3 and 880 cm^{-1} for K_2CO_3), but this is not observed. The Ca^{2+} for K^+ ion exchange scenario would be in agreement with the EPMA analysis of the 50% OMW-2 loaded CaT-Z, showing a reduced Ca and a significantly increased K content after adsorption. However, due to experimental constraints, the ATR spectral range does not extend to the FIR region, where the Ca and K cation motion can be distinguished at ca. 250 cm^{-1} (Yiannopoulos et al. 2001) and 140 cm^{-1} (Kamitsos and Risen Jr 1984), respectively.

The 1018 cm^{-1} composite band downshift to ca. 1011 cm^{-1} for the 50% OMW-1 loaded CaT-Z and the 50% OMW-2 loaded NZ sample is difficult to reconcile with the absence of changes observed in the minerals of the 50% OMW-1 loaded CaT-Z in the XRD patterns. Since the orthophosphate incorporation in all samples is expected to be minimal (see the EPMA results for 50% OMW-2 loaded CaT-Z, i.e., 0.01–0.05 P_2O_5 wt%, Table 4), the apparent downshift cannot be attributed to a contribution from the $\nu_3(\text{PO}_4^{3-})$ asymmetric stretch, as has been done in the case of a much richer phosphate-containing wastewater like fresh urine (0.80–1.06 P_2O_5 wt%, see Table S1 in earlier study (Mitrogiannis et al. 2018)). The appearance of the 780- cm^{-1} shoulder in 50% OMW-2 loaded NZ and 50% OMW-1 loaded CaT-Z could

be attributed to the incorporation of K_2O in the silicate matrix, which is known to cause a small downshift of the Si–O–Si bridge bending vibrations with respect to the usual silicate Na_2O environment, but this cannot explain the downshift of the strong ca. 1011- cm^{-1} composite band which would be expected to upshift with K_2O content (Kamitsos and Risen Jr 1984). The absence of the shoulder at 780 cm^{-1} in 50% OMW-2 loaded CaT-Z, can be explained by assuming that practically all of the potassium ions are adsorbed as calcite-type K_2CO_3 in this sample instead of partly being incorporated in the silicate phase as well.

Finally, the O–H stretching infrared bands of adsorbed water/structural hydroxyl in the inset of Fig. 9 do not show any appreciable changes, in contrast to the case of adsorbed ammonium ions where N–H stretching vibrations were also assigned (Mitrogiannis et al. 2018).

Conclusions

Two different samples of anaerobically digested and diluted OMW were treated with $\text{Ca}(\text{OH})_2$ modified zeolite, focusing on P and K removal. A comparative adsorption test showed a higher P removal efficiency by CaT-Z than by NZ. In both OMW samples, phosphate anions and potassium cations were simultaneously adsorbed on CaT-Z. The maximum experimental adsorption capacity of CaT-Z for K (12.75 and 15.76 mg/g in 50% OMW-1 and OMW-2, respectively) was higher than that for phosphate P (1.08 and 2.14 mg/g) due to the much higher initial concentrations of K in the OMW samples. The measured values of the adsorbed total organic carbon (TOC) (0.37 and 1.47 mg/g) showed that CaT-Z displayed a higher selectivity for dissolved K and P than for OMW organic matter. However, the proportion of adsorbed TOC to adsorbed P is significant, ranging from 34.2 to 68.7%. Therefore, the total alkalinity and dissolved organic matter in OMW samples seem to have a negative influence on phosphate adsorption. Sequential desorption tests revealed that the plant-available P is the main fraction of adsorbed P on CaT-Z contacted with OMW-1 and OMW-2. The co-occurrence of Ca and P as well as the increase of P and K contents at the zeolitic matrix of CaT-Z after the adsorption is confirmed by the results of the qualitative X-ray maps and Electron Probe Micro-analysis, respectively. The latter in situ technique indicated that solute K ions were exchanged mainly with Ca and less with Mg ions on CaT-Z. The ATR-IR analysis revealed alterations in the functional groups of loaded CaT-Z which are related to the K adsorption and suggest a Ca^{2+} to K^+ ion exchange among the surface carbonate groups. The present study demonstrated positive results for the recovery of favorable OMW compounds. Further studies are needed in respect

of increasing the removal percentage of P and K from undiluted OMW using higher CaT-Z dosages or other adsorbents and investigating the potential usage of spent adsorbents as soil amendment enriched with plant-available nutrients.

Acknowledgements Part of this research (D. Mitrogiannis, Assist. Prof. M. Psychoyou, Dr. M. Brulé) was financed by the General Secretariat of Research and Technology (Greece) in the frame of EranetMed BIOGASMENA project (ID 72-026) entitled “Demonstration of dry fermentation and optimization of biogas technology for rural communities in the MENA (Middle East and North Africa) region”. Professor M. Kornaros was funded by the General Secretariat of Research and Technology (GSRT, Greece) in the frame of the BIOSOL project (ERANETMED_ENERG-11-75, Grant Agreement No. 609475, MIS T3EPA-00047) “Development and demonstration of a Hybrid CSP-biomass gasification boiler System”. D. Palles and E.I. Kamitsos acknowledge support of the project “National Infrastructure in Nanotechnology, Advanced Materials and Micro-/Nanoelectronics” (MIS 5002772) which is implemented under the Action “Reinforcement of the Research and Innovation Infrastructure,” funded by the Operational Programme “Competitiveness, Entrepreneurship and Innovation” (NSRF 2014-2020) and co-financed by Greece and the European Union (European Regional Development Fund)

References

- Achak M, Hafidi A, Ouazzani N, Sayadi S, Mandi L (2009a) Low cost biosorbent “banana peel” for the removal of phenolic compounds from olive mill wastewater: kinetic and equilibrium studies. *J Hazard Mater* 166:117–125
- Achak M, Mandi L, Ouazzani N (2009b) Removal of organic pollutants and nutrients from olive mill wastewater by a sand filter. *J Environ Manag* 90:2771–2779
- Aharonov-Nadborny R, Tsechansky L, Raviv M, Graber E (2018) Mechanisms governing the leaching of soil metals as a result of disposal of olive mill wastewater on agricultural soils. *Sci Total Environ* 630:1115–1123
- Akhiar A, Battimelli A, Torrijos M, Carrere H (2017) Comprehensive characterization of the liquid fraction of digestates from full-scale anaerobic co-digestion. *Waste Manag* 59:118–128
- Al-Malah K, Azzam MO, Abu-Lail NI (2000) Olive mills effluent (OME) wastewater post-treatment using activated clay. *Sep Purif Technol* 20:225–234
- Aly AA, Hasan YN, Al-Farraj AS (2014) Olive mill wastewater treatment using a simple zeolite-based low-cost method. *J Environ Manag* 145:341–348
- Aly AA, Alashgar KN, Al-Farraj AS, Ibrahim HM (2018) Contaminants and salinity removal of olive mill wastewater using zeolite nanoparticles. *Sep Sci Technol* 53:1638–1653
- APHA (1999) Standard methods for the examination of water and wastewater. American Public Health Association, American Water Works Association, Water Environment Federation, Washington DC
- Arienzo M, Christen E, Jayawardane N, Quayle WC (2012) The relative effects of sodium and potassium on soil hydraulic conductivity and implications for winery wastewater management. *Geoderma* 173:303–310
- Azzam MO (2018) Olive mills wastewater treatment using mixed adsorbents of volcanic tuff, natural clay and charcoal. *J Environ Chem Eng* 6:2126–2136
- Barbera AC, Maucieri C, Cavallaro V, Ioppolo A, Spagna G (2013) Effects of spreading olive mill wastewater on soil properties and crops, a review. *Agric Water Manag* 119:43–53
- Blika P, Stamatelatos K, Kornaros M, Lyberatos G (2009) Anaerobic digestion of olive mill wastewater. *Global NEST Journal* 11:364–372
- Chen X, Wendell K, Zhu J, Li J, Yu X, Zhang Z (2012) Synthesis of nano-zeolite from coal fly ash and its potential for nutrient sequestration from anaerobically digested swine wastewater. *Bioresour Technol* 110:79–85
- Dareioti MA, Dokianakis SN, Stamatelatos K, Zafiri C, Kornaros M (2009) Biogas production from anaerobic co-digestion of agroindustrial wastewaters under mesophilic conditions in a two-stage process. *Desalination* 248:891–906
- Frascardi D, Bacca AEM, Zama F, Bertin L, Fava F, Pinelli D (2016) Olive mill wastewater valorisation through phenolic compounds adsorption in a continuous flow column. *Chem Eng J* 283:293–303
- Guaya D, Hermassi M, Valderrama C, Farran A, Cortina JL (2016) Recovery of ammonium and phosphate from treated urban wastewater by using potassium clinoptilolite impregnated hydrated metal oxides as N-P-K fertilizer. *J. Environ. Chem. Eng.* 4:3519–3526
- Han C, Wang Z, Yang W, Wu Q, Yang H, Xue X (2016) Effects of pH on phosphorus removal capacities of basic oxygen furnace slag. *Ecol Eng* 89:1–6
- Hopkinson L, Rutt KJ, Kristova P (2018) The near-infrared spectra of the alkali carbonates. *Spectrochim Acta A Mol Biomol Spectrosc* 200:143–149
- Howell C, Myburgh P (2018) Management of winery wastewater by re-using it for crop irrigation—a review. *S Afr J Enol Vitic* 39:116–131
- Inglezakis VJ, Pouloupoulos SG, Kazemian H (2018) Insights into the S-shaped sorption isotherms and their dimensionless forms. *Microporous Mesoporous Mater* 272:166–176
- Inglezakis VJ, Fyrrillas MM, Park J (2019) Variable diffusivity homogeneous surface diffusion model and analysis of merits and fallacies of simplified adsorption kinetics equations. *J Hazard Mater* 367:224–245
- Kamitsos EI, Risen WM Jr (1984) Vibrational spectra of single and mixed alkali pentasilicate glasses. *J Non-Cryst Solids* 65:333–354
- Kamitsos E, Karakassides M, Patsis A (1989) Spectroscopic study of carbonate retention in high-basicity borate glasses. *J Non-Cryst Solids* 111:252–262
- Khoufi S, Louhichi A, Sayadi S (2015) Optimization of anaerobic co-digestion of olive mill wastewater and liquid poultry manure in batch condition and semi-continuous jet-loop reactor. *Bioresour Technol* 182:67–74
- Kocatürk-Schumacher NP, Bruun S, Zwart K, Jensen LS (2017a) Nutrient recovery from the liquid fraction of digestate by clinoptilolite. *CLEAN—Soil, Air, Water* 45:1500153
- Kocatürk-Schumacher NP, Zwart K, Bruun S, Brussaard L, Jensen LS (2017b) Does the combination of biochar and clinoptilolite enhance nutrient recovery from the liquid fraction of biogas digestate? *Environ Technol* 38:1313–1323
- Kontos S, Koutsoukos P, Paraskeva C (2014) Removal and recovery of phenolic compounds from olive mill wastewater by cooling crystallization. *Chem Eng J* 251:319–328
- Kougias P, Kotsopoulos T, Martzopoulos G (2014) Effect of feedstock composition and organic loading rate during the mesophilic co-digestion of olive mill wastewater and swine manure. *Renew Energy* 69:202–207
- Koutsos T, Chatzistathis T, Balampekou E (2018) A new framework proposal, towards a common EU agricultural policy, with the best sustainable practices for the re-use of olive mill wastewater. *Sci Total Environ* 622:942–953

- Lin L, Wan C, Lee D-J, Lei Z, Liu X (2014) Ammonium assists ortho-phosphate removal from high-strength wastewaters by natural zeolite. *Sep Purif Technol* 133:351–356
- Loganathan P, Vigneswaran S, Kandasamy J, Bolan NS (2014) Removal and recovery of phosphate from water using sorption. *Crit Rev Environ Sci Technol* 44:847–907
- Makris KC, El-Shall H, Harris WG, O'Connor GA, Obreza TA (2004) Intraparticle phosphorus diffusion in a drinking water treatment residual at room temperature. *J Colloid Interface Sci* 277:417–423
- Malamis S, Katsou E (2013) A review on zinc and nickel adsorption on natural and modified zeolite, bentonite and vermiculite: examination of process parameters, kinetics and isotherms. *J Hazard Mater* 252–253:428–461
- Maragkaki A, Vasileiadis I, Fountoulakis M, Kyriakou A, Lasaridi K, Manios T (2018) Improving biogas production from anaerobic co-digestion of sewage sludge with a thermal dried mixture of food waste, cheese whey and olive mill wastewater. *Waste Manag* 71: 644–651
- Markou G, Mitrogiannis D, Inglezakis V, Muylaert K, Koukouzas N, Tsoukalas N, Kamitsos E, Palles D, Baziotis I (2018) Ca(OH)₂ pre-treated bentonite for phosphorus removal and recovery from synthetic and real wastewater. *CLEAN–Soil, Air, Water* 46:1700378
- Mitrogiannis D, Psychoyou M, Baziotis I, Inglezakis VJ, Koukouzas N, Tsoukalas N, Palles D, Kamitsos E, Oikonomou G, Markou G (2017) Removal of phosphate from aqueous solutions by adsorption onto Ca(OH)₂ treated natural clinoptilolite. *Chem Eng J* 320:510–522
- Mitrogiannis D, Psychoyou M, Koukouzas N, Tsoukalas N, Palles D, Kamitsos E, Pantazidis A, Oikonomou G, Baziotis I (2018) Phosphate recovery from real fresh urine by Ca(OH)₂ treated natural zeolite. *Chem Eng J* 347:618–630
- Naidu G, Jeong S, Choi Y, Song MH, Oyunchuluun U, Vigneswaran S (2018) Valuable rubidium extraction from potassium reduced seawater brine. *J Clean Prod* 174:1079–1088
- Pantziaros AG, Jaho S, Karga I, Iakovides IC, Koutsoukos PG, Paraskeva CA (2018) Struvite precipitation and COD reduction in a two-step treatment of olive mill wastewater. *J Chem Technol Biotechnol* 93: 730–735
- Scoma A, Bertin L, Zanaroli G, Fraraccio S, Fava F (2011) A physicochemical–biotechnological approach for an integrated valorization of olive mill wastewater. *Bioresour Technol* 102:10273–10279
- Świąteczak P, Cydzik-Kwiatkowska A, Zielińska M (2019) Treatment of the liquid phase of digestate from a biogas plant for water reuse. *Bioresour Technol* 276:226–235
- Tsigkou K, Sakarika M, Komaros M (2019) Inoculum origin and waste solid content influence the biochemical methane potential of olive mill wastewater under mesophilic and thermophilic conditions. *Biochem Eng J* 151:107301
- Víctor-Ortega MD, Ochando-Pulido JM, Airado-Rodríguez D, Martínez-Férez A (2016) Experimental design for optimization of olive mill wastewater final purification with Dowex Marathon C and Amberlite IRA-67 ion exchange resins. *J Ind Eng Chem* 34:224–232
- Wan C, Ding S, Zhang C, Tan X, Zou W, Liu X, Yang X (2017) Simultaneous recovery of nitrogen and phosphorus from sludge fermentation liquid by zeolite adsorption: mechanism and application. *Sep Purif Technol* 180:1–12
- Wijesinghe DTN, Dassanayake KB, Scales P, Sommer SG, Chen D (2018) Removal of excess nutrients by Australian zeolite during anaerobic digestion of swine manure. *J Environ Sci Health A* 53: 362–372
- Worch E (2012) Adsorption technology in water treatment: fundamentals, processes, and modeling. Walter de Gruyter
- Yang M, Lin J, Zhan Y, Zhu Z, Zhang H (2015) Immobilization of phosphorus from water and sediment using zirconium-modified zeolites. *Environ Sci Pollut Res* 22:3606–3619
- Yiannopoulos Y, Chryssikos GD, Kamitsos E (2001) Structure and properties of alkaline earth borate glasses. *Phys Chem Glasses* 42:164–172
- Zagklis DP, Arvaniti EC, Papadakis VG, Paraskeva CA (2013) Sustainability analysis and benchmarking of olive mill wastewater treatment methods. *J Chem Technol Biotechnol* 88:742–750
- Zagklis DP, Vavouraki AI, Komaros ME, Paraskeva CA (2015) Purification of olive mill wastewater phenols through membrane filtration and resin adsorption/desorption. *J Hazard Mater* 285:69–76
- Zhu B-Y, Gu T (1989) General isotherm equation for adsorption of surfactants at solid/liquid interfaces. Part 1. Theoretical. *Journal of the Chemical Society, Faraday Transactions 1: Physical Chemistry in Condensed Phases* 85:3813–3817
- Zhu B-Y, Gu T (1991) Surfactant adsorption at solid-liquid interfaces. *Adv Colloid Interf Sci* 37:1–32

Publisher's note Springer Nature remains neutral with regard to jurisdictional claims in published maps and institutional affiliations.